Hierarchical Modeling of Heat Transfer in Silicon-Based Electronic Devices

Javier V. Goicochea
Department of Mechanical Engineering,
Carnegie Mellon University,
Pittsburgh, PA 15213

Marcela Madrid
Pittsburgh Supercomputing Center,
Pittsburgh, PA 15213

Cristina Amon
Department of Mechanical and Industrial Engineering,
University of Toronto,
ON, M5S 1A4, Canada

A hierarchical model of heat transfer for the thermal analysis of electronic devices is presented. The integration of participating scales (from nanoscale to macroscales) is achieved by (i) estimating the input parameters and thermal properties to solve the Boltzmann transport equation (BTE) for phonons using molecular dynamics (MD), including phonon relaxation times, dispersion relations, group velocities, and specific heat, (ii) applying quantum corrections to the MD results to make them suitable for the solution of BTE, and (iii) numerically solving the BTE in space and time subject to different boundary and initial conditions. We apply our hierarchical model to estimate the silicon out-of-plane thermal conductivity and the thermal response of an silicon on insulator (SOI) device subject to Joule heating. We have found that relative phonon contribution to the overall conductivity changes as the dimension of the domain is reduced as a result of phonon confinement. The observed reduction in the thermal conductivity is produced by the progressive transition of modes in the diffusive regime (as in the bulk) to transitional and ballistic regimes as the film thickness is decreased. In addition, we have found that relaxation time expressions for optical phonons are important to describe the transient response of SOI devices and that the characteristic transport regimes, determined with Holland and Klemens phonon models, differ significantly. [DOI: 10.1115/1.4001644]

1 Introduction

The performance and reliability of modern electronic devices, such as microprocessors, is related to their ability to dissipate the heat generated from their operation. However, as their characteristic dimensions become comparable to or smaller than the mean free path or the relaxation time of the main energy carriers, the thermal conductivity of the constituent materials decreases from their bulk values. At subcontinuum scales, the interactions of the energy carriers become a fundamental part in the description of the heat transport. Lower values of thermal conductivity restrict heat dissipation and induce large thermal stresses and temperature changes. In semiconductor materials, these interactions are described in terms of quantized lattice vibrations or phonons [1]. Phonons are subject to complex collisions or scattering mechanisms (e.g., phonon-phonon, phonon-impurities, phonon-boundaries, and phonon-defects), which play a crucial role in describing how the heat is transported in the crystalline structure [2,3].

To model the thermal behavior of these devices, considering all scales involved, is a complex task. The complexity lies in the large variation in the participating spatial (from nanometers to centimeters) and temporal scales (from picoseconds to hours) in their intricate operation and in the physical behavior and nature of each scale. Even though the formulation of the thermal transport at the subcontinuum level has long been established [1–5], no mathematical method is able to fully resolve by itself the thermal response of electronic devices from nanoscale to macroscales. For instance, molecular dynamics (MD), which is a classical method, is essentially constrained to small (submicro) scales due to the expensive computations involved. The Boltzmann transport equation (BTE) on the other hand requires input parameters such as the relaxation time of phonons, which are difficult to estimate [6–10]. Likewise, the Fourier law, which is valid only at the macroscopic level, assumes instantaneous heat propagation and ignores interactions among phonons. From these methods, the solution of BTE under the single mode relaxation time (SMRT), approximation offers the possibility to model the heat transport from subcontinuum scales to continuum scales if the required phonons relaxation times are available.

There are several problems associated with the analytical estimation of the relaxation time of phonons. First, phenomenological models (derived from perturbation theory) are not reliable outside the range for which their parameters were fitted [11,12] and the effect of the approximations involved in their derivation (such as isotropic crystal, elastic continuum behavior, piecewise linear dispersion relations, third-order anharmonic expansions, etc.) are shadowed by the use of fitting parameters [13]. Second, since the relative contribution of the acoustic (A) and optical (O) and transverse (T) and longitudinal (L) phonons to the total thermal conductivity in semiconductors is still an open topic, these relaxation time models are not accurate. For instance, recent *ab initio* [14] and MD predictions obtained using the Stillinger–Weber (SW) potential for silicon [15] suggest that the contribution of acoustic modes is approximately 90–95% depending on the temperature of the system being the contribution of transverse acoustic (TA) about 30%. However, these results contrast with analytical estimations from Holland [4] and Hamilton and Parrott [16] who suggested that the TA modes were the dominant heat carriers at high temperatures. Sood and Roy [17] concluded that longitudinal acoustic (LA) phonons dominate heat transport in germanium at high temperatures being the contribution of the LA phonons more than 75% for $T > \theta_D$. Third, there is a lack of relaxation time expressions applicable to optical modes and frequently thermal estimations neglected their contribution. Different authors [7,18–20] have pointed out that optical phonons can have a significant effect on the creation of hotspots during transient Joule heating events due to the confinement of phonons, which can severely impact the operation temperature of silicon on insulator (SOI) devices. Notable are the works of Sinha et al. [18], Pop and co-workers [21,22], and, more recently, Rowlette and Goodson [6], who studied the scattering mechanisms of longitudinal optical (LO) phonons at hotspots and developed nonequilibrium electron and electron-phonon transport models, respectively, applicable to

Contributed by the Heat Transfer Division of ASME for publication in the JOURNAL OF HEAT TRANSFER. Manuscript received May 8, 2008; final manuscript received April 13, 2010; published online July 23, 2010. Assoc. Editor: Jayathi Murthy.

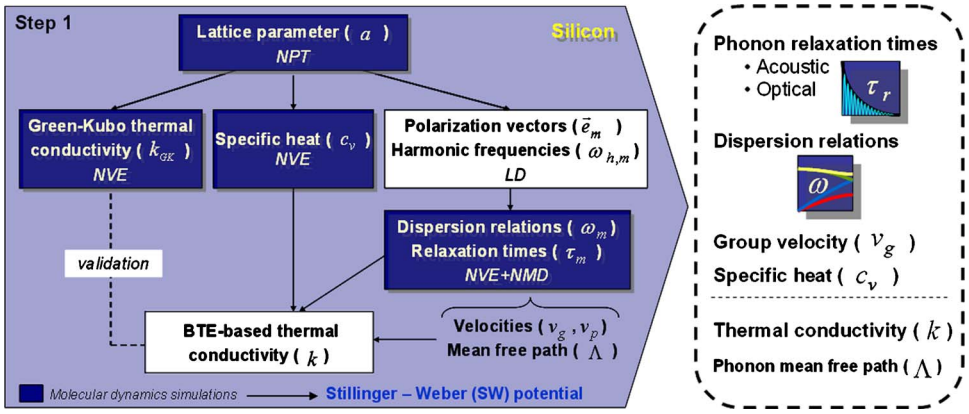

Fig. 1 Step 1: Estimation of different properties and relaxation times with MD

nanometer-scale field-effect transistors. Lastly, the accuracy of common relaxation time models in more complex semiconductors is unknown.

In this work, we present a hierarchical model of heat transfer for the thermal analysis of electronic devices. In the proposed methodology, the phonon relaxation times and the dispersion relations of silicon are estimated by means of MD simulations, removing in this way the need of fitting parameters. The methodology considers the effect of the anharmonicity of the potential energy function over the thermal expansion of the crystal and the change in the dispersion, which are particularly difficult to include in theoretical derivations [23] and might be important in systems, where the phonon vibration frequencies are expected to change significantly with temperature [24]. In addition, no explicit simplifications about the lattice structure or the contribution of anharmonic terms are required as it is commonly needed in theoretical derivations.

The integration of participating scales is achieved in three steps. First, we use MD simulations to estimate the properties required to solve the BTE for phonons. In the second step, we apply quantum corrections (QCs) to the MD results to make them suitable for BTE. This is required since MD and BTE interpret the physics of phonons differently. Lastly, we solve the BTE using these properties. Here, we use the SW potential to describe the interactions between silicon atoms and we solve the BTE using the lattice Boltzmann method (LBM) under the SMRT approximation. We apply our methodology to analyze the out-of-plane thermal conductivity and the thermal response of a SOI-like device subject to Joule heating.

2 Methodology

Our final goal is to numerically solve in space and time the BTE for phonons using the properties estimated from MD including phonon relaxation times ($\tau_{r,m}$), dispersion relations (ω_m), group velocity ($\boldsymbol{v}_{g,m}$), and specific heat (c_v). Under the SMRT approximation, the BTE can be written as follows:

$$\frac{\partial f_m}{\partial t} + \boldsymbol{v}_{g,m} \cdot \nabla f_m = -\frac{f_m - f_m^o}{\tau_{r,m}} \tag{1}$$

In the equation, f_m and f_m^o are the current and equilibrium distribution functions and t is the time. Phonons follow the equilibrium distribution function given by the Bose–Einstein distribution.

$$f_m^o = \left\{ \exp\left[\frac{\hbar \omega_m}{k_B T} \right] - 1 \right\}^{-1} \tag{2}$$

where $\hbar$ and k_B represent the Plank and Boltzmann constants and T is the equilibrium temperature.

We solve the BTE with the LBM using an isotropic and dispersive phonon formulation. The formulation includes acoustic and optical phonons (with longitudinal and transverse polarizations) whose properties depend on frequency. Details of the solution of the BTE using the LBM are presented in Appendix. In order to obtain the inputs needed to solve the BTE, first, we perform MD simulations using an NPT ensemble (constant number of atoms, pressure, and temperature) to determine the lattice parameter of silicon at 300 K and 1000 K. In this way, we consider the thermal expansion of the crystal. Then, as detailed below (see Fig. 1), we proceed to determine all other phonon properties using the lattice parameters obtained previously. For this, we perform additional MD simulations using an NVE ensemble (constant number of atoms, volume, and energy). For both ensembles, the instantaneous position and velocity of atoms are obtained by solving Newton's second law.

$$M \frac{d^2 \boldsymbol{r}}{dt^2} = \boldsymbol{F} \tag{3}$$

where M is the atom's mass, $\boldsymbol{r}$ is the position of the atom in the molecular domain, t represents the time, and $\boldsymbol{F}$ is the force.

The phonon relaxation times are computed from the energies obtained in the MD simulation using the normal mode decomposition method; specifically from the temporal decay of the autocorrelation function of the energy of each mode (m), where the energy of each mode is a function of the instantaneous position and velocity of each atom. This procedure was first proposed by Ladd et al. [25] and extended by McGaughey and Kaviany [24] for the determination of the phonon relaxation times and thermal conductivity of LJ argon under the isotropic approximation. Sun and Murthy [26], Henry and Chen [27], and, more recently, Goicochea et al. [15] used the environment-dependent interatomic potential (EDIP) and the SW potential to determine the relaxation times of silicon. Additionally, Turney et al. [28] presented four different methods for predicting phonon properties and thermal conductivity of argon based on lattice dynamics, on molecular dynamics, and on the solution Boltzmann transport equation. Their results indicate that the shape of the spectral thermal conductivity is closely related to the density of phonon states and that phonons with a frequency of half the maximum frequency are found to dominate thermal transport.

Under the harmonic approximation, the total energy of each mode can be written as [29]

$$E_{m,t} = \frac{\omega_{h,m}{}^2 Q_m^*(\boldsymbol{q},\lambda) Q_m(\boldsymbol{q},\lambda)}{2} + \frac{\dot{Q}_m^*(\boldsymbol{q},\lambda) \dot{Q}_m(\boldsymbol{q},\lambda)}{2} \tag{4}$$

where $\omega_{h,m}$ is the harmonic frequency and the first and second terms on the right hand side of the equation represent the potential energy and kinetic energy of the mode m, respectively. $Q_m(\boldsymbol{q},\lambda)$ is the normal mode of the system [29] given by

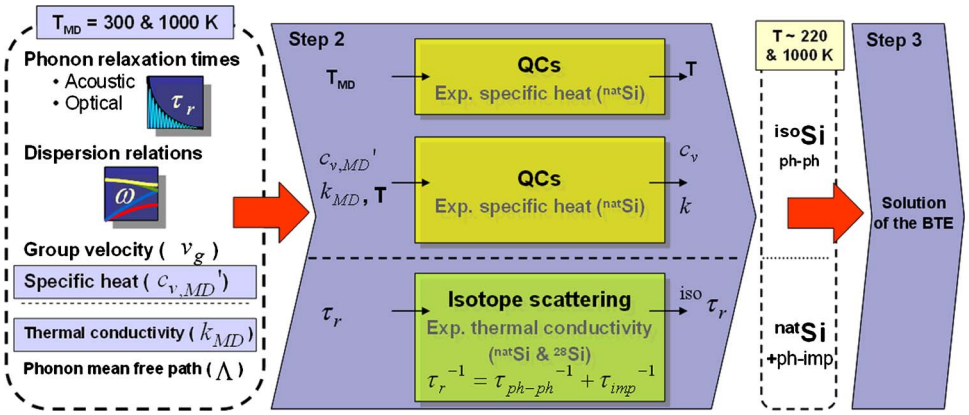

Fig. 2 Steps 2 and 3: Quantum correction of MD properties and solution of the BTE

$$Q_m(\boldsymbol{q},\lambda) = N^{-1/2}\sum_i M_i^{1/2}\exp(-\boldsymbol{q}\cdot\boldsymbol{r}_{i,0})\boldsymbol{e}_m^*(\boldsymbol{q},\lambda)\cdot\boldsymbol{u}_i(t) \quad (5)$$

where N is the number of atoms, M_i is the mass of atom i, and λ corresponds to the mode polarization (longitudinal or transverse) described by the polarization vector $\boldsymbol{e}_m^*(\boldsymbol{q},\lambda)$, i.e., its complex conjugate. $\boldsymbol{r}_{i,0}$ is the equilibrium position of atom i, and $\boldsymbol{u}_i(t)$ is the relative displacement of atom i at time t from its equilibrium position $(\boldsymbol{u}_i(t)=\boldsymbol{r}_i(t)-\boldsymbol{r}_{i,0})$.

Once the total energy $E_{m,t}$ of each mode is obtained for each time step in the MD simulation, the autocorrelation of the deviation of total energy from its mean value $(\delta E_{m,t}=E_{m,t}-\bar{E}_m)$ is computed. The normalized autocorrelation produces a temporal decaying function that is fitted with an exponential function from which the relaxation time of mode m is extracted.

Likewise, the dispersion relations $\omega_m(\boldsymbol{q},\lambda)$ can be directly determined using the equipartition theorem between the kinetic and potential energy of each mode.

$$\omega_m(\boldsymbol{q},\lambda) = \sqrt{\frac{\langle\dot{Q}_m(\boldsymbol{q},\lambda)\dot{Q}_m(-\boldsymbol{q},\lambda)\rangle}{\langle Q_m(\boldsymbol{q},\lambda)Q_m(-\boldsymbol{q},\lambda)\rangle}} \quad (6)$$

Once the dispersion relations are obtained, the group and phase velocities are obtained as $v_g=\partial\omega/\partial q$ and $v_p=\omega/q$. The specific heat is computed using the procedures reported in Refs. [30,31]. We validate the MD obtained properties by comparing the silicon bulk thermal conductivity determined using the Green–Kubo method (k_{GK}) and that obtained from the steady state solution of the BTE (i.e., the thermal conductivity expression of Tiwari and Agrawal [32], which corresponds to the expression between curly brackets in Eq. (9)) at the studied temperatures.

Since MD is a classical method, before solving the BTE, the temperature, specific heat, and thermal conductivity have to be quantum corrected. This is particularly important at temperatures below the Debye temperature. (i.e., 645 K for Si [33]). Several strategies have been proposed to quantum correct the thermal conductivity and temperature [34–36]. We use the method proposed in Ref. [34], which includes the experimental specific heat to quantum correct both quantities. In addition, as explained below, we have extended this method to correct the thermal conductivity per phonon mode. In Ref. [34], the thermal conductivity is corrected as

$$k = \frac{dT_{\mathrm{MD}}}{dT}\{k_{\mathrm{MD}}\} \rightarrow k = \frac{c_{v,e}(T)}{3(N-1)k_B}\{k_{\mathrm{MD}}\} \quad (7)$$

where dT_{MD}/dT is defined as the ratio between the experimental $(c_{v,e})$ and the classical specific heat $(3(N-1)k_B)$. Likewise, the corrected temperature (T) is found integrating Eq. (7) as

$$T_{\mathrm{MD}}(T) = \frac{V}{3(N-1)k_B}\int_0^T c_{v,e}(T)dT + T^* \quad (8)$$

where T^* is the integration constant of the order of the Debye temperature [34].

To include the quantization of the energy of each mode at T and the change in the dispersion relations, we modify Eq. (7), considering that the corrected thermal conductivity is a function of the mode contribution to the specific heat $c_{v,a}(T,\omega)$, temperature, and of the ration between the total experimental and analytical specific heats $(c_{v,e}(T)/c_{v,a}(T))$

$$k = \frac{c_{v,e}(T)}{c_{v,a}(T)}\left\{\frac{4\pi}{3}\frac{1}{(2\pi)^3}\sum_{b,p}\left[\int_{\omega_{m,\min}}^{\omega_{m,\max}}\left(c_{v,a}(T,\omega)\frac{v_g}{v_p{}^2}\tau_r\right)\omega^2 d\omega\right]\right\} \quad (9)$$

For simplicity, the summation is performed in the [100] direction over all phonon branches and polarizations, where the relaxation times are determined. In Eq. (9), we assume that the crystal is isotropic, however, no changes are needed if an anisotropic model is considered. Lastly, the MD specific heat is corrected as $c_v(T,\omega)=c_{v,e}(T)c_{v,\mathrm{MD}}{}'(c_{v,a}(T,\omega)/c_{v,a}(T))$, where $c_{v,\mathrm{MD}}{}'$ is the MD specific heat per degree of freedom. $c_{v,\mathrm{MD}}{}'$ is 1.01 and 1.05 at 300 K and 1000 K, respectively.

To validate the second step of our methodology, we compare our estimated thermal conductivity with that obtained experimentally for natural Si ($^{\mathrm{nat}}$Si). For this, the isotope scattering is included in our phonon-phonon relaxation times ($\tau_{\mathrm{ph-ph}}$). In silicon, the isotope scattering is only important at temperatures approximately below 350 K [37]. $^{\mathrm{nat}}$Si has three stable isotopes (different forms of an element each having different atomic mass): ^{28}Si, ^{29}Si, and ^{30}Si in a proportion of 92.23%, 4.67%, and 3.1%, respectively. We include the phonon-isotope relaxation times (τ_{imp}) using an expression obtained from perturbation theory. The phonon-isotope relaxation times are included using Matthiessen's rule ($\tau_r{}^{-1}=\tau_{\mathrm{ph-ph}}{}^{-1}+\tau_{\mathrm{imp}}{}^{-1}$). Alternatively, the effect of isotope scattering can be modeled explicitly with MD using silicon atoms with different masses [38]. Klemens [2] and Carruthers [39] suggested two expressions for this type of scattering. Both of them are used to study the effect of isotope scattering.

$$\tau_{\mathrm{imp}}{}^{-1} = A\omega^4 \quad \text{and} \quad \tau_{\mathrm{imp}}{}^{-1} = Av_g{}^{-3}\omega^4 \quad (10)$$

where A is a fitted constant.

As shown in Fig. 2, the inclusion of the isotope scattering results in two sets of properties. One includes only phonon-phonon scattering ($^{\mathrm{iso}}$Si) and another includes the scattering with isotopes

Table 1 Relative contribution of each mode to the overall thermal conductivity at 300 K and 1000 K

From	T	$\frac{c_v}{k_B}$	k_{TA}	k_{LA}	k_{LO}	k_{TO}	k_{MD}	k_{GK}	A
MD	300	1.01	122.8 (33.87%)	202.590 (55.87%)	34.186 (9.43%)	2.953 (0.82%)	362.5	350.67	
+QC	220	See Sec. 2	119.656 (38.62%)	172.518 (55.67%)	16.530 (5.33%)	1.163 (0.38%)	309.9		
+ISO $A\omega^4$	220		116.186 (43.79%)	143.747 (53.83%)	6.004 (2.19%)	0.518 (0.19%)	265.3		1.57×10^{-45} (s^3/rad^4)
+ISO $\frac{A}{v_g^3}\omega^4$	220		107.750 (40.62%)	153.554 (57.88%)	3.973 (1.50%)	0.021 (0.01%)	265.3		2.47×10^{-34} (m^3/rad^4)
MD	1000	1.05	18.0 (29.99%)	35.385 (58.88%)	6.240 (10.38%)	0.438 (0.73%)	60.092		52.36

T is the temperature in (K), c_v/k_B is the nondimensional specific heat per unit of degree of freedom, k_{TA}, k_{LA} k_{LO} k_{TO} are the thermal conductivity contribution of the transverse and longitudinal acoustic and optical modes, respectively, k_{MD} is the BTE-based thermal conductivity obtained from MD results, and k_{GK} is the Green–Kubo thermal conductivity. MD, +QC, +ISO are the from molecular dynamics, after quantum corrections, and after isotope scattering, respectively. Thermal conductivity values in (W/m K).

(^{nat}Si). After these properties are quantum corrected, the BTE for phonons is solved and the methodology is applied to the study cases.

3 Results

In this section, results pertained to each of the steps of our hierarchical model are presented. Due to length considerations and since the first and second steps of the methodology have been presented individually [15,40,41], more emphasis is provided to the application of the methodology. For completeness, we also discuss the most important results found in the first two steps.

3.1 Step 1: Thermal Properties Estimation. We have found that the behavior of the phonon relaxation times for the different modes can be well-captured using power functions of the form: $1/\tau_r = a\omega^b$ [15]. At both temperatures the value of the exponents of the power functions for the acoustical modes (TA and LA) are approximately equal to 2 [15], which is in agreement with the theoretical predictions obtained from time-dependent perturbation theory for U-processes at high temperatures [3]. For optical modes, the value of the exponents is higher than 2, indicating that higher-order processes might be responsible for such behavior (as suggested in Ref. [15]).

It is observed that the anharmonic nature of the potential energy and the thermal expansion are responsible for the change in the dispersion relations with temperature. The change in the frequency of vibration is noticeable in the transverse modes, however, their change is relatively small compared with that obtained for argon [24] using the normal mode decomposition.

Table 1 shows the values obtained for specific heat and thermal conductivities of the TA, LA, LO, and transverse optical (TO) modes. As expected, the obtained specific heat is approximately k_BT. The small derivation from the classical specific heat at 1000 K is produced due to the anharmonic nature of the potential energy function. The relative contribution is obtained from the expression Tiwari and Agrawal considering that the specific heat is constant. At 300 K and 1000 K, we have found that the contribution of the TA and LA modes represents roughly 90% being about 30% from the TA mode and lower than 60% from the LA mode while the relative contribution of LO mode is 10%. The contribution from the TO mode for both temperatures is negligible (less 1%). In addition, both predictions match the overall thermal conductivity obtained with Green–Kubo. The difference between both thermal conductivities $(k-k_{GK})/k^*_{GK}100$ is 3.39% and 14.76% at 300 K and 1000 K, respectively. Both values fall within one standard deviation of the predicted values of the Green–Kubo method (i.e., 4.90% (17.38 W/m K) and 21.13% (11.16 W/m K) at 300 K and 1000 K, respectively). The agreement between these values validates the properties obtained with MD in this step. Furthermore, recent results for Ge [42] obtained using MD at high temperature agree very well with these predictions.

3.2 Step 2: Quantum Corrections and Isotope Scattering. Table 2 shows the QC temperatures calculated from Eq. (8) and using the experimental specific heat corresponds to that for natural silicon (^{nat}Si) [43]. In addition, due to the lack of experimental data for single Si isotopes and for comparison purposes, the temperature is also corrected replacing the experimental specific heat by the corresponding analytical expression (Eq. (11)).

$$c_{v,a}(T) = \sum_m \left\{ k_B(\hbar\omega_m/k_BT)^2 \frac{\exp(\hbar\omega_m/k_BT)}{[\exp(\hbar\omega_m/k_BT)-1]^2} \right\} \quad (11)$$

The frequency values used in Eq. (11) are those obtained from Eq. (6). Note that both estimations (experimental and analytical) provide similar results. At 300 K, the corrected temperature is roughly 220 K while at 1000 K, the correction is negligible (less than 1.2%). The analytical estimations are obtained for T^* = 790.94 K.

The QCs also affect the behavior of the specific heat with frequency. Figure 3 shows the mode specific heat as a function frequency at T_{MD}=300 K. Before QCs, the specific heat is independent of the frequency of vibration of the modes, however, when the quantization of the energy is considered, the specific heat decreases as the frequency is increased. The quantum corrected specific heat starts at almost the same value of the corresponding for the classical anharmonic system, however, the difference becomes larger at higher frequencies. The small shift in the specific heat values observed at zero-frequency is produced due to the difference between the experimental and the analytic specific heats $(c_{v,e}(T)/c_{v,a}(T))$. The freezing of high-frequency modes translates in a reduction in their contribution to the overall thermal conductivity. As shown in Table 1, the relative contribution of the optical modes reduces from 10.25% before QCs to 5.70% after QCs while the one from acoustical modes increases from 89.75% to 94.30%.

To include the effect of isotope scattering, we find the value of A (in Eq. (10)) that produces the reduction in the experimental

Table 2 Quantum corrected temperatures

	T	
T_{MD}	Experimental	Analytical
300	218.5	220.6
1000	1011.3	1006.5

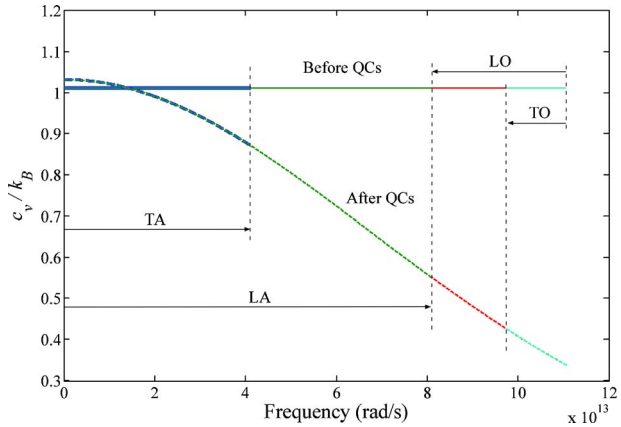

Fig. 3 Mode specific heat after quantum corrections. Arrows indicate the frequency range of each mode.

thermal conductivity due to isotope scattering. Based on experimental data reported by Kremer et al. [37] for ^{nat}Si and ^{28}Si (i.e., silicon enriched with isotope 28) at $T=220$ K, we estimate that such reduction (measured relatively to the ^{nat}Si thermal conductivity) is 16.80%.

As shown in Fig. 4, the inclusion of the isotope scattering term modifies the phonon relaxation times and all properties that depend on them (e.g., phonon mean free path, thermal conductivity, etc.). In particular, the phonon mean free path decreases as the frequency of each mode increases being the reduction more severe for high-frequency modes (i.e., LO and TO modes) and when the group velocity is considered in the phonon-impurity scattering term. Additionally, the relative contribution of high-frequency modes to the thermal conductivity is modified. As reported in Table 1, the contribution of optical modes reduces to less than 2.4% while the one from the acoustical modes increases to more than 97.6% when the first expression in Eq. (10) is used. Note that although both isotope scattering expressions yield to the same value of thermal conductivity, the reduction in the contribution of optical modes occurs regardless of the expression used for the phonon-isotope scattering. When the second expression of Eq. (10) is used, the contribution of TO modes becomes negligible.

3.2.1 Comparison With Experimental Data. Table 3 shows the comparison between the predicted thermal conductivity with that obtained experimentally for ^{nat}Si and ^{28}Si. The deviation of the predicted thermal conductivity before and after QCs are applied

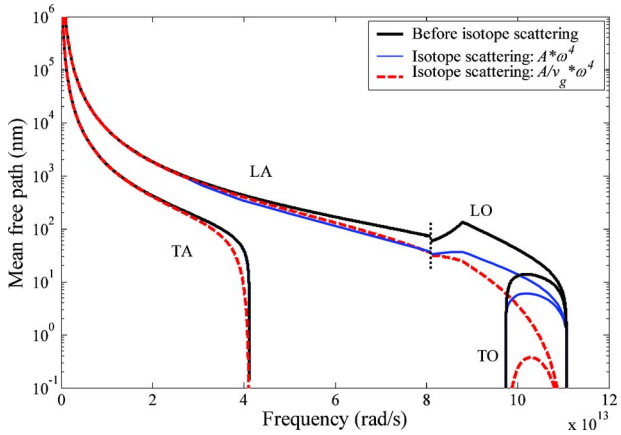

Fig. 4 Effect of the isotope scattering term in the phonon mean free path. The thin dotted line presents the edge of the BZ.

Table 3 Thermal conductivity comparison before and after isotope scattering with experimental data

From	k	$\left\lvert \frac{k}{k_e(^{28}\mathrm{Si})} - 1 \right\rvert$	$\left\lvert \frac{k}{k_e(^{nat}\mathrm{Si})} - 1 \right\rvert$
MD	362.5	44.48%	
+QC	309.9	23.48%	
+ISO	265.3		13.94%

$k_e(^{28}\mathrm{Si})=250.934$ W/m K [37], $k_e(^{nat}\mathrm{Si})=232.844$ W/m K [44], and k_e is the experimental thermal conductivity.

with respect to the experimental value is 44.48% and 23.48% for ^{28}Si. When the isotope scattering term is included, a deviation of 13.94% is found between our thermal conductivity predictions and the experimental value for ^{nat}Si. Hence, both the proposed quantum correction and the inclusion of the isotope scattering term improve the thermal conductivity predictions.

3.2.2 High Temperature Implications. At high temperatures, both the quantization of the energy and the presence of isotopes are expected to have a minor effect on the reduction in the thermal conductivity. Although there are no reported values of thermal conductivity for ^{28}Si at 1000 K, it is well known that at high temperatures phonon-phonon scattering is the main source of thermal resistance. It is interesting to note that the contribution to the thermal conductivity from the high-frequency modes would approach the ones estimated with MD (before QCs) as the temperature of the system is increased.

3.3 Step 3: Solution of the BTE and Study Cases. In this section, we discuss the results of the application of the methodology. Details of the solution of the BTE using the LBM are presented in Appendix. We apply the methodology to estimate the silicon out-of-plane thermal conductivity and the thermal response of an SOI device subject to Joule heating. The calculated phonon dispersion relations, specific heat, group velocity, and relaxation times are provided as input to solve the BTE.

3.3.1 Out-of-Plane Thermal Conductivity. The out-of-plane thermal conductivity is obtained for a thin film of thickness d. It is assumed that the length L of the film is several times larger than its thickness $L \gg d$. The film is modeled as a one-dimensional domain (see Fig. 5) with prescribed temperature at the top and bottom boundaries. All other boundaries are assumed to be adiabatic and no phonon-boundary scattering is possible with them. The procedure to determine the out-of-plane thermal conductivity is described in Ref. [45].

Figure 6 shows the out-of-plane thermal conductivity obtained with ^{nat}Si and ^{iso}Si at 220 K. For comparison, the out-of-plane conductivity obtained with relaxation times models of Escobar et al. [46] (i.e., gray formulation), Holland [4], and Han and Klemens [47]. In general, all conductivity curves have the same behavior; they approach their bulk values as the thickness increases. At 100 nm and 1000 nm, the difference between ^{nat}Si and ^{iso}Si is 15% and 23%, respectively. This is expected, since the bulk thermal conductivity of ^{iso}Si is higher than that for ^{nat}Si (see Table 3). Note that despite Holland [4] and Han and Klemens [47] models were designed to reproduce the bulk thermal conductivity of sili-

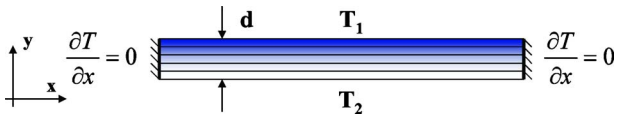

Fig. 5 One-dimensional domain used to estimate the out-of-plane thermal conductivity

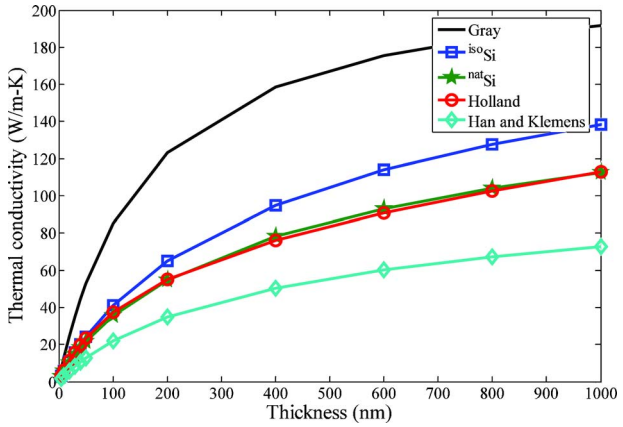

Fig. 6 Silicon thin film out-of-plane thermal conductivity as a function of film thickness at 220 K

con over a wide range of temperatures, their predictions obtained for the studied thicknesses differ significantly. Furthermore, despite 220 K the out-of-plane conductivity obtained with the Holland model is higher than that of the Han and Klemens model, the situation reverses at 1000 K for film thickness below 100 nm. Coincidentally, at 220 K Holland model predicts similar out-of-plane conductivities as those obtained with ^{nat}Si.

In Fig. 6, all phonon models have thermal conductivity values lower than that for the gray formulation. This is produced due to the transition of phonon modes from the diffusive transport regime to the ballistic regime as the thickness of the film reduces. This transition, observed in our LBM dispersive formulations, has been *qualitatively* explained due to the coexistence of different phonons [7]. Different transport regimes originate due to the existence of frequency-dependent phonons with different relaxation times, group velocities, and, hence, different mean free paths. For a given characteristic dimension of the film, this yield to phonons with different Knudsen number (Λ/d) coexisting in the same phonon system. A similar behavior has been previously observed in Ref. [7].

To elucidate this effect, Fig. 7 shows the frequency-dependent Knudsen number for a film of 1000 nm at 220 K and 1000 K. At both temperatures, only low-frequency TA and LA modes fall within the ballistic regime region at both temperatures. The rest of the LA modes are located in the transitional region. This is also the situation for the TA modes, except for those modes with higher frequency. At 1000 K most of the LO and TO modes are located in the diffusive region, however, at 220 K the low-frequency LO modes also fall within the transitional region. In general, the increase in temperature produces that more modes are locate within the transitional and diffusive regions, which corresponds to a decrease in the phonon mean free path for all modes and thermal conductivity. Contrarily, further reductions in the thickness will increase the number of modes falling within the ballistic and transitional regions, especially low-frequency modes. For phonons falling within the transitional and ballistic regimes, the phonon-boundary scattering becomes a major source of thermal resistance, reducing their contribution to the thermal conductivity.

The evidence of change in the contribution of the different modes to the thermal conductivity as a function of the thickness is shown in Fig. 8. In the figure, the variation in mode thermal conductivity of ^{iso}Si as a function of film thickness is shown. The mode thermal conductivity is determined for three different films of increasing thickness from 100 nm to 10000 nm and is calculated expressing Eq. (9) as

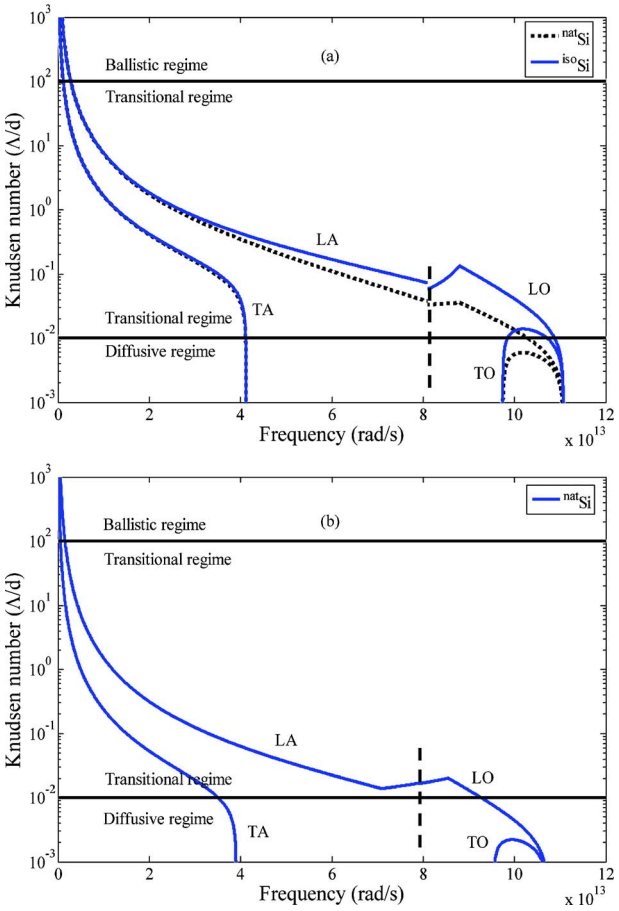

Fig. 7 Variation in Knudsen number with respect to frequency for a film thickness of 1000 nm at 220 K (*a*) and 1000 K (*b*). The dashed line represents the edge of the BZ.

$$k = \sum_m \int_{\omega_{m,\min}}^{\omega_{m,\max}} k_m(\omega) d\omega \tag{12}$$

where the summation includes all branches and polarizations. Again an isotropic phonon space is assumed.

As shown in Fig. 8, the increase in the film thickness not only affects the mode contribution to the thermal conductivity (especially for those low-frequency modes) but the peaks for the TA

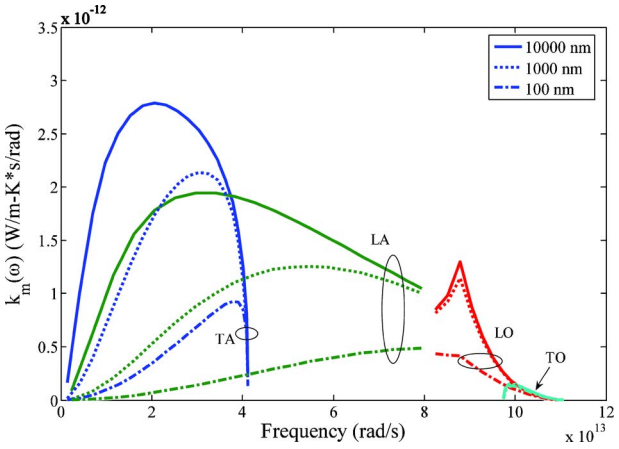

Fig. 8 Variation in mode thermal conductivity as a function of film thickness at 220 K

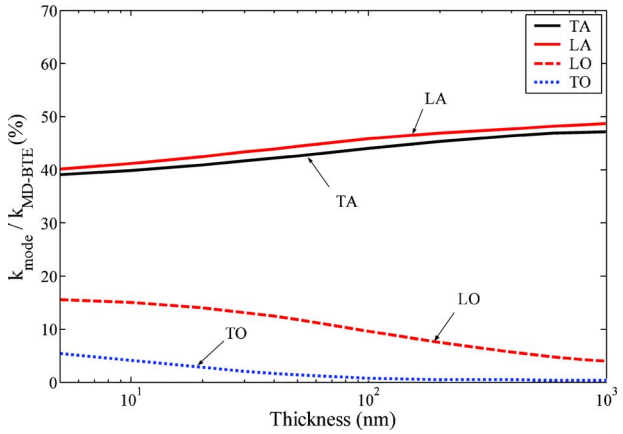

Fig. 9 Mode thermal conductivity contribution as a function of thickness

and LA modes are progressively displaced to the left. In the limit of a large film thickness (previously estimated to be of the order of millimeters [7,48]), the location of the peaks and the contribution of the low-frequency modes would correspond to that of the bulk case, as reported in Table 1. For small thicknesses the relative contribution of the modes to the overall thermal conductivity changes significantly due to phonon confinement.

Figure 9 shows how the contribution of the TA, LA, LO, and TO modes to the overall thermal conductivity changes as a function of film thickness for ^{nat}Si. For films of 10 nm, acoustical modes contribute about 80% while optical modes contribute 20%, being 15% and 5% the contribution of the LO and TO modes, respectively. This represents a substantial increase in the contribution of the optical modes from the bulk values (see Table 1). The behavior is also present in ^{iso}Si, where optical modes contribute about 22% for a 10 nm film and in the phonon relaxation time models of Holland and Han and Klemens (not shown). In Holland model, the contribution of the TA and LA modes decreases from 58.3% and 41.7% for bulk to 24.5% and 75.5% while in Han and Klemens model the contribution of the TA and LA modes changes from 33.0% and 67.0% for bulk to 24.4% and 75.6% at 10 nm and 220 K. To the best of our knowledge, this is the first time that this change in the thermal conductivity is quantitatively reported for Si.

3.3.2 Thermal Response of a SOI Device. The thermal response of a SOI device is modeled by considering a one-dimensional silicon layer of $L=100$ nm subject to self-heating. The heat generation occurs at the center of the domain in a region 1/10 smaller than the length of the silicon layer, as shown in Fig. 10. The top and bottom boundaries are considered adiabatic. Temperatures at the right and left boundaries are maintained at a constant value. The value of the phonon relaxation times depends on the initial temperature of the film. It is considered that the silicon layer is fabricated of ^{nat}Si and ^{iso}Si.

To study the thermal response of the SOI device, we analyze the transient behavior of temperature at the center of the hotspot. Pop et al. [21] determined phonon emission and energy dissipation rates, due to Joule heating, using a coupled electron-phonon

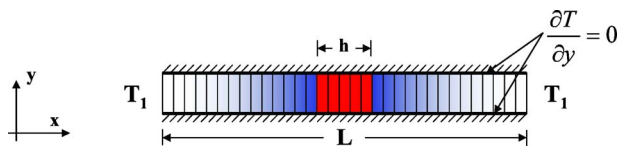

Fig. 10 One-dimensional domain used to model the silicon layer of a SOI transistor

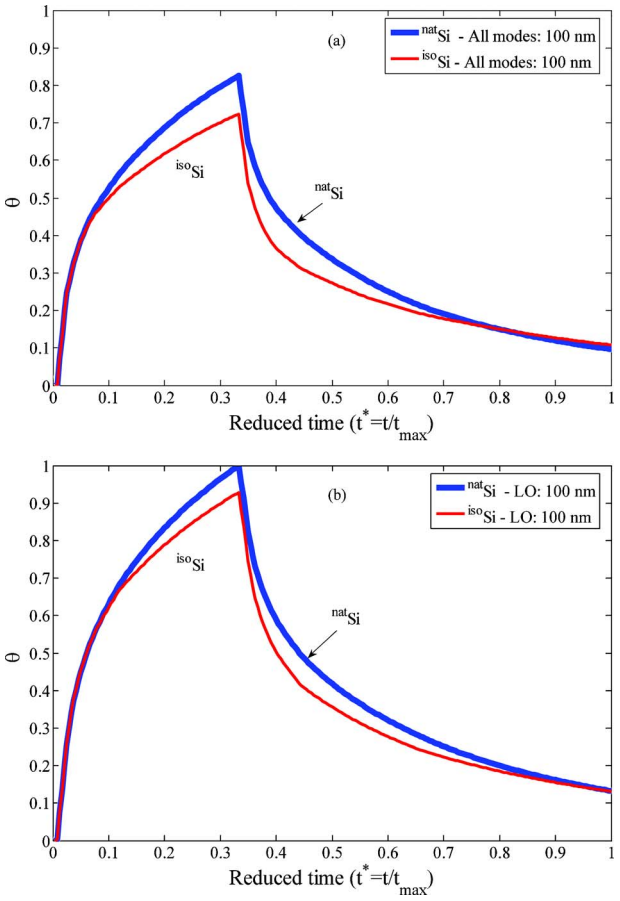

Fig. 11 Temperature evolution at the center of the hotspot for a film of 100 nm. (*a*) Heat generated is distributed over all phonon modes, (*b*) Heat generated is distributed only in LO mode.

model. Here, we use their results to model how the total heat generated due to the operation of the SOI device under low and high electric fields (5 kV/cm and 50 kV/cm) is distributed among the heat carriers. When a high electric field is applied, all heat generated is distributed in the LO, LA, and TO modes with a ratio about 1/2, 1/3, and 1/10, respectively. Conversely, for the low electric field case, all heat is distributed in the LO mode [21]. The same amount of heat is dissipated in both scenarios (i.e., 10×10^{12} W/cm^3). Figure 11 shows the nondimensionalized temperature as a function of time at the center of the hotspot subject to high and low electric fields. The temperature and thickness of the film have been nondimensionalized as $\theta=(T-T_{min})/(T_{max}-T_{min})$ and $\xi=x/d$, where T_{min} initial temperature inside of the layer and T_{max} is the maximum temperature found during all simulations. Likewise, the time scale is defined as $t^*=t/t_{max}$, where t and t_{max} are the actual and total simulation time, respectively. The total simulation time (t_{max}) is 60 ps and the heat pulse last 1/3 of the total time.

In the figure, an increase in the temperature during the first 20 ps is observed. The maximum peak temperature is found when the heat pulse is applied to ^{nat}Si and all the heat is distributed in the LO mode. This is produced due to the low thermal conductivity of the LO mode for which the isotope scattering further reduces the contribution of optical modes.

The temperature behavior of ^{iso}Si shows two characteristic effects of ballistic heat transport [7]. First, the slope of the temperature as a function of time during the application of the heat pulse is slower than for ^{nat}Si, especially for $t^*>0.1$. Second, despite the higher thermal conductivity of ^{iso}Si, its rate of cooling is lower

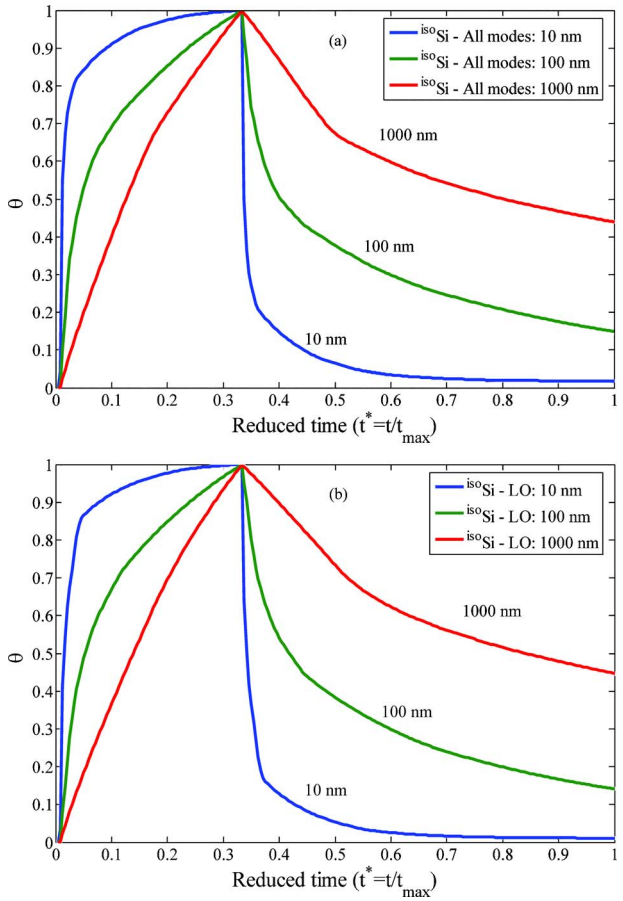

Fig. 12 Temperature evolution at the center of the hotspot for different film thicknesses. Hotspot size is 1/10 of the thickness of the film. Heat generated is distributed over all phonon modes (*a*) and through the LO mode (*b*).

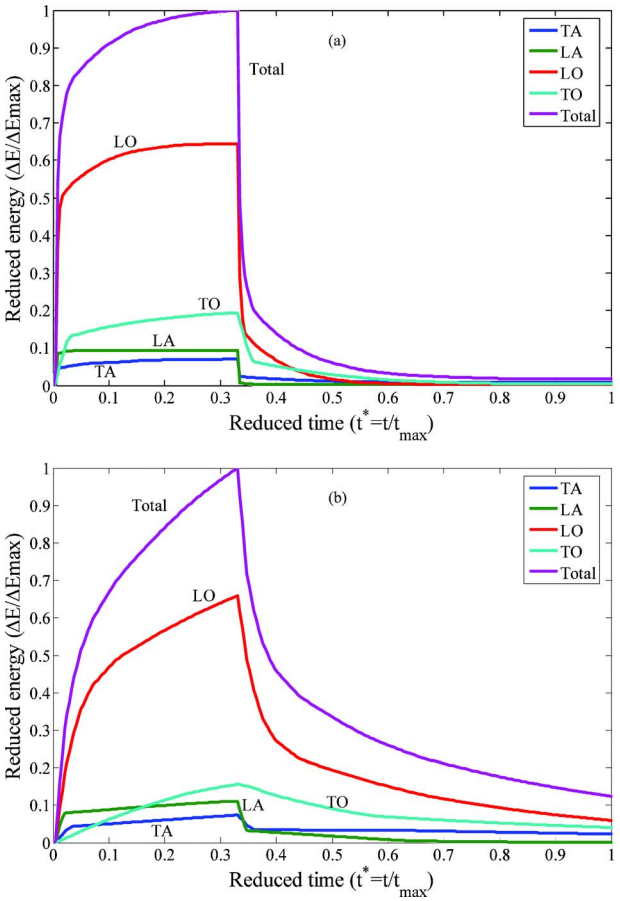

Fig. 13 Contribution of the TA, LA, LO, and TO modes to the reduced phonon total energy as a function of reduced time for films thicknesses of 10 nm (*a*) and 100 nm (*b*)

than that for ^{nat}Si. For ^{iso}Si, when the heat pulse is turned off, the temperature decreases rapidly followed by a slower rate of cooling. These effects are less noticeable in ^{nat}Si since more phonons fall within the transitional or diffusive regimes (Fig. 7(*a*)).

Figure 12 shows the temperature evolution at the center of the hotspot for film thicknesses of 10 nm, 100 nm, and 1000 nm and ^{iso}Si subject also the high and low electrical fields. For films of 1000 nm, the temperature increases roughly linear while the heat pulse is on, followed by a slow cooling rate. This behavior is characteristic of diffusive heat transport [7,48] and is essentially independent of how the generated heat is distributed among phonon modes. As the film thickness is reduced, the transient evolution of temperature changes. For 100 nm films, the hotspot increases more rapidly until $t^* < 0.1$ (approximately) followed by a reduction in the temperature slope. Then, when the heat pulse is turned off, the hotspot temperature reduces rapidly. Further reductions in the film thickness accentuate this behavior. For 10 nm films, the heating and cooling of the hotspot occurs abruptly. Initially, the increase in temperature is steep until it becomes almost flat, followed by quickly temperature drop produced after the heat pulse is turned off. A similar behavior in the hotspot temperature was observed by Escobar and Amon [7]. Similar temperature changes are also found for ^{nat}Si.

Figure 13 shows the change in the reduced energy (Eq. (13)) of each phonon branch and polarization as a function of the reduced time for films thicknesses of (a) 10 nm and (b) 100 nm. All generated heat is assumed distributed among all modes as described previously. The film is fabricated of ^{iso}Si. The reduced energy is defined as

$$\left(\frac{\Delta E}{\Delta E\ \max}\right)^t = \frac{E_p^t - E_p^{t=0}}{E_{\text{total}}^t - E_{\text{total}}^{t=0}} \tag{13}$$

where E_p^t is energy of each phonon branch and polarization (i.e., TA, LA, LO, and TO), E_{total}^t is the total energy of all phonons, and the superscript t represents the time.

The shape of the total energy curves follows the same behavior as the hotspot temperature (shown in Fig. 12(*a*)) for equivalent film thicknesses. Despite the heat generated is distributed among all modes, the contribution of each mode to the total energy varies significantly. Acoustic modes follow a similar trend to that observed in Fig. 12(*a*) for a film thickness of 10 nm (which is characteristic of ballistic transport [7]). These modes experience an abrupt change in their energy levels as the heat pulse is turned on or off since they fall in the ballistic and transitional regimes (see Fig. 7(*a*)). For both thicknesses, the LA mode is more excited than the TA mode. This is produced because 1/3 of the heat generated is transferred through the LA mode. On the other hand, the low thermal conductivity of optical modes produces a large increase in their energy levels, leading to phonon confinement. Phonon confinement is further promoted due to the distribution of 1/2 and 1/10 of the total heat generated into the LO and TO modes, respectively. For a film of 100 nm the energy of optical modes increases with a lower rate than for acoustic modes while the heat pulse is on, followed by a slower cooling rate. It can be verified that for a film of 100 nm, most optical phonons fall in the transitional and diffusive regimes. As the film thickness is reduced to 10 nm, most optical phonons fall in the transitional regime and the behavior approaches that of ballistic transport. Evidently, the behavior of the total phonon energy and temperature at the hotspot

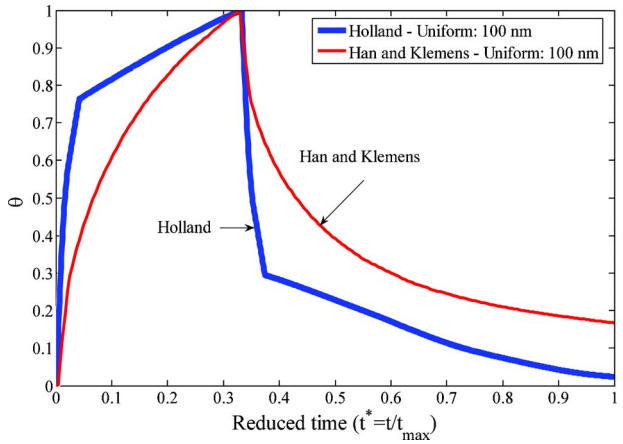

Fig. 14 Temperature at the center of the hotspot for a film of 100 nm as a function of time, obtained from Holland, and Han and Klemens phonon relaxation times models

are strongly affected by the confinement of optical modes.

Figure 14 compares the temperature at the center of the hotspot for a film of 100 nm obtained from Holland and Han and Klemens. In this case, all heat generated is distributed uniformly among the TA and LA modes. From the figure, the thermal predictions of both models differ drastically. Holland's model predict a behavior similar to that of ballistic transport while Han and Klemens' predict a hotspot temperature behavior similar to the transitional regime, resembling that obtained for ^{nat}Si for the same film thickness. As expected, the maximum temperature at the hotspot depends on the phonon model used. Holland's model predicts the lowest hotspot temperature, followed in increasing order by ^{iso}Si, ^{nat}Si, and Han and Klemens (which has the lowest thermal conductivity). The presence of optical modes in ^{iso}Si and ^{nat}Si increase their thermal resistance due to phonon confinement leading to higher temperatures at the hotspot.

4 Summary and Conclusions

A hierarchical modeling methodology for heat transfer of silicon-based electronic devices has been presented. The integration of participating scales has been achieved in three steps. These involve (i) the estimation of the thermal properties at different temperatures required to solve the BTE, including phonon relaxation times, dispersion relations, group velocity, and specific heat, (ii) their quantum correction to make them suitable for BTE, and (iii) the solution of this equation using an isotropic and dispersive lattice Boltzmann formulation for phonons. Nonlinear dispersion relations in the [100] direction for the acoustic and optical modes (longitudinal and transverse) were used to solve the BTE. The different steps of the methodology were validated using analytic or experimental data reported in literature.

It is found that the reduction in the out-of-plane conductivity is produced by a progressive transition of modes from diffusive regimes (as in the bulk case) to transitional or ballistic regime regions as the film thickness is reduced. This transition is characterized by a shift in the location of the mode thermal conductivity peaks for the acoustic modes as the film thickness is reduced, which at the same time modifies the relative contribution of all modes to the thermal conductivity. For ^{nat}Si and ^{iso}Si, the total contribution of the optical modes increases to 20% and 22% when the film thickness is reduced to 10 nm. At this thickness, the LO and TO modes contribute about 15% and 5% to the thermal conductivity, respectively. Similar changes are also found in the LA and TA modes for the models of Holland and Han and Klemens.

The thermal response of SOI-like transistors of decreasing size is characterized by temperature profiles that become progressively nonlinear. The transition to ballistic transport is observed as both the length and the hotspot size decreases. The hotspot temperature exhibits abrupt changes as the heat pulse is turned on or off, produced due to the sudden changes in the energy levels of each mode. It was found that acoustic modes dissipate the generated heat ballistically, whereas the behavior of optical modes is identified to be within the transitional and diffusive regimes. Under self-heating conditions, acoustic modes exhibit a saturation of their energy levels as the heat pulse is turned on while those of optical modes increase due to their lower thermal conductivity. The difference between transient behavior of temperature (in nondimensional units) obtained for ^{nat}Si and ^{iso}Si is not substantially different, however, notable differences are found using the models of Holland and Han and Klemens.

The value of hierarchical methodology stands out when the results obtained from different phonon relaxation time models are compared. Despite Holland and Han and Klemens, the models are able to reproduce the silicon bulk thermal conductivity, their predictions for out-of-plane thermal conductivity, and behavior of temperature at the hotspot differ drastically. The difference in the results obtained from Holland and Han and Klemens models reaffirms the importance of our proposed methodology, which can be extended to other semiconductor materials and to validate models for phonon relaxation times.

Acknowledgment

The authors gratefully acknowledge the funding of the National Science Foundation under Grant No. CTS-0103082 and the Pennsylvania Infrastructure Technology Alliance (PITA), a partnership of Carnegie Mellon, Lehigh University, and the Commonwealth of Pennsylvania's Department of Community and Economic Development (DCED). Most of the computations were performed on the National Science Foundation Terascale Computing System at the Pittsburgh Supercomputing Center under Grant No, CTS-070003P.

Nomenclature

A = fitted coefficient (s^3/rad^4 or m^3/rad^4)
c_v/k_B = nondimensional specific heat per degree of freedom
$c_{v,e}$ = experimental specific heat (kg/s^2 K)
$c_{v,a}$ = analytic specific heat (kg/s^2 K)
$c_{v,a}(T,\omega)$ = mode contribution to the specific heat as a function of temperature and frequency
d = silicon layer thickness (nm)
E_p^t = energy of each phonon branch and polarization (J)
E_{total}^t = total energy of all phonons (J)
f_m = phonon distribution function
$\hbar$ = Plank constant (J*s/rad)
k_e = experimental thermal conductivity (W/m K)
$k_e(^{28}\text{Si})$ = experimental thermal conductivity of enriched 28 silicon (W/m K)
$k_e(^{nat}\text{Si})$ = experimental thermal conductivity of natural silicon (W/m K)
k = quantum corrected thermal conductivity (W/m K)
k_B = Boltzmann constant (kg/s^2 K)
k_{GK} = Green–Kubo thermal conductivity (W/m K)
k_{MD} = BTE-based thermal conductivity (W/m K)
$k_m(\omega)$ = mode thermal conductivity as a function of frequency (W/m K*s/rad)
L = silicon layer length (nm)
N = number of atoms
q = wave vector (1/m)
Si = Silicon
t = time (s)

T = temperature (K)
T_{MD} = molecular temperature (K)
T^* = integration constant (K)
v_g, v_p = group and phase velocities (m/s)
w_m = LBM weighting factor

Greek Symbols

θ = nondimensional temperature
θ_D = Debye temperature (K)
Δx = lattice spacing
Δt = time step
Λ = mean free path (nm)
τ_m = relaxation time (s)
ω = frequency (rad/s)

Superscripts

O = equilibrium
* = nondimensional

Subscripts

m = phonon mode
max = maximum
min = minimum
TA, LA = transverse and longitudinal acoustics
TO, LO = transverse and longitudinal opticals

Appendix

LBM is a computational method originally developed for fluid simulation [49]. In this method, the spatial domain is discretized in lattices that only have a finite number of propagation directions. Since all our simulations are one-dimensional, we use the D1Q3 lattice [50], considering only two propagation directions (left and right). On each lattice, a discretized version of the BTE known as the lattice Boltzmann kinetic equation (LBKE) is solved. The latter was obtained after applying two different operators to the first and second terms on the right of Eq. (1): one forward in time (t) and one forward in time and space (x), respectively. One important characteristic of the LBM is that the lattice spacing and time are linked by the so-called light-cone rule [49] (i.e., $\Delta x = v^* \Delta t$). This results in Eq. (A1) (w_m is a weighting factor defined as $w_m = \Delta x / (|v_{g,m}| \tau_m) = \Delta t / \tau_m$).

$$f_{m,i}(x + dx, t + dt) = (1 - w_m) f_{m,i}(x,t) + w_m f^o_{m,i}(x,t) \qquad \text{(A1)}$$

In our dispersive LBM phonon formulation, multiple LBKEs are solved simultaneously in space and time. One equation per phonon is defined in the simulation domain [7]. Phonons are obtained from the discretization of the dispersion relations in bands of constant wave vector [7] or constant frequency [9]. This leads to phonon properties (e.g., group velocities) that depend on frequency. In our case, our dispersion relations obtained in the [100] direction are discretized using constant wave vector bands and all phonon properties are band-average with respect to frequency (i.e., $\bar{\alpha} = 1/\Delta\omega \int_{\Delta\omega} \alpha(\omega) d\omega$). Unlike a gray model [46], which include only a single phonon with one group velocity, in a dispersive formulation many phonons are defined.

The solution of each LBKE in space and time follows the next algorithm: (i) given a finite number of phonons defined in the simulation, the initial temperature of the system and its boundary conditions, we use Eq. (2) to obtain the initial phonon distribution functions in the domain. Since the temperature at the boundaries is typically prescribed, the equilibrium distribution at these locations for each phonon defined remains fixed during the entire simulation; (ii) multiple equations, such as Eq. (A1), are solved and (iii) at the end of each time step, the total phonon energy is computed on each lattice site and a new temperature distribution is obtained using Eq. (2). Steps ii and iii are repeated until the predefined simulation time is reached.

In the algorithm, it is implicitly assumed that the energy of the phonon system remains in quasi-equilibrium. Hence, the temperature of the system can be recovered from equilibrium distribution functions. In this way, all our results are strictly valid in the limit of low normal modes amplitudes. The impact of this approximation was discussed in Ref. [15]. Other nonequilibrium phonon formulation to solve BTE has been developed [6,10,21].

To maintain the accuracy at an acceptable level while keeping the computational effort at minimum, the sensitivity of the bulk thermal conductivity at 220 K to the number of bands (per branch) used to discretize the dispersion relations was evaluated. The sensitivity is defined as $[k(n_w) - k(n_w - 1)]/k(n_w)$, where k is the thermal conductivity and n_w is the number of bands per branch. For $n_w = 10$ or 40, the phonon defined (i.e., ten bands * four branches) the sensitivities of 3.7%, 5.2%, 0.03%, and 0.04% were found using the models of Holland, Han, and Klemens and for ^{nat}Si and ^{iso}Si, respectively. Additionally, since the LBM is a nonconservative method, the sensitivity with respect to the spatial discretization was also evaluated. All our results are independent of the number of cells used to discretize the domain. However, it is important to mention that the number of cells we use to discretize the domain varies with the domain size. The light-cone rule restriction is particularly severe in multiphonon systems, especially for phonons whose group velocity approach to zero (i.e., transverse modes near the BZ edge) and therefore the number of cell used is generally large enough for the results to be independent of spatial discretization [41]. Mesh independence was found with a minimum of 800 cells. For the film of 10,000 nm (see Fig. 8), approximately 30,000 cell were used.

References

[1] Peierls, R. E., 1955, *Quantum Theory of Solid*, Oxford University Press, London.
[2] Klemens, P. G., 1958, "Thermal Conductivity and Lattice Vibrational Modes," *Solid State Physics*, F. Seitz and D. Thurnbull, eds., Academic, New York, pp. 1–98.
[3] Klemens, P. G., 1969, "Theory of Thermal Conductivity of Solids," *Thermal Conductivity*, R. P. Tye, ed., Academic, London, pp. 1–68.
[4] Holland, M. G., 1963, "Analysis of Lattice Thermal Conductivity," Phys. Rev., **132**(6), pp. 2461–2471.
[5] Ziman, J., 1960, *Electrons and Phonons: The Theory of Transport Phenomena in Solids*, Oxford University Press, Oxford, UK.
[6] Rowlette, J., and Goodson, K., 2008, "Fully Coupled Nonequilibrium Electron–Phonon Transport in Nanometer-Scale Silicon FETs," IEEE Trans. Electron Devices, **55**(1), pp. 220–232.
[7] Escobar, R., and Amon, C. H., 2007, "Influence of Phonon Dispersion on Transient Thermal Response of Silicon-on-Insulator Transistors Under Self-Heating Conditions," ASME J. Heat Transfer, **129**(7), pp. 790–797.
[8] Mazumder, S., 2001, "Monte Carlo Study of Phonon Transport in Solid Thin Films Including Dispersion and Polarization," ASME J. Heat Transfer, **123**(4), pp. 749–759.
[9] Narumanchi, S. V. J., Murthy, J. Y., and Amon, C. H., 2005, "Comparison of Different Phonon Transport Models for Predicting Heat Conduction in Silicon-on-Insulator Transistors," ASME J. Heat Transfer, **127**(7), pp. 713–723.
[10] Narumanchi, S. V. J., Murthy, J. Y., and Amon, C. H., 2004, "Submicron Heat Transport Model in Silicon Accounting for Phonon Dispersion and Polarization," ASME J. Heat Transfer, **126**(6), pp. 946–955.
[11] Kazan, M., Pereira, S., Coutinho, J., Correia, M. R., and Masri, P., 2008, "Role of Optical Phonon in Ge Thermal Conductivity," Appl. Phys. Lett., **92**(21), p. 211903.
[12] Holland, M. G., 1964, "Phonon Scattering in Semiconductors From Thermal Conductivity Studies," Phys. Rev., **134**(2A), pp. A471–A480.
[13] Chung, J. D., McGaughey, A. J. H., and Kaviany, M., 2004, "Role of Phonon Dispersion in Lattice Thermal Conductivity Modeling," ASME J. Heat Transfer, **126**(3), pp. 376–380.
[14] Broido, D. A., Malorny, M., Birner, G., Mingo, N., and Stewart, D. A., 2007, "Intrinsic Lattice Thermal Conductivity of Semiconductors From First Principles," Appl. Phys. Lett., **91**(23), p. 231922.
[15] Goicochea, J. V., Madrid, M., and Amon, C. H., 2010, "Thermal Properties for Bulk Silicon Based on the Determination of Relaxation Times Using Molecular Dynamics," ASME J. Heat Transfer, **132**(1), p. 012401.
[16] Hamilton, R. A., and Parrott, J. E., 1969, "Variational Calculation of the Thermal Conductivity of Germanium," Phys. Rev., **178**(3), pp. 1284–1292.
[17] Sood, K. C., and Roy, M. K., 1993, "Longitudinal Phonons and High-Temperature Heat Conduction in Germanium," J. Phys.: Condens. Matter, **5**(3), pp. 301–312.
[18] Sinha, S., Schelling, P. K., Phillpot, S. R., and Goodson, K. E., 2005, "Scattering of G-Process Longitudinal Optical Phonons at Hotspots in Silicon," J. Appl. Phys., **97**(2), p. 023702.
[19] Narumanchi, S. V. J., Murthy, J. Y., and Amon, C. H., 2006, "Boltzmann

Transport Equation-Based Thermal Modeling Approaches for Hotspots in Microelectronics," Heat Mass Transfer, **42**(6), pp. 478–491.
[20] Pop, E., Banerjee, K., Sverdrup, P., Dutton, R., and Goodson, K., 2001, "Localized Heating Effects and Scaling of Sub-0.18 Micron CMOS Devices," IEEE Int. Electron Dev. Meet., pp. 677–680.
[21] Pop, E., Dutton, R. W., and Goodson, K. E., 2005, "Monte Carlo Simulation of Joule Heating in Bulk and Strained Silicon," Appl. Phys. Lett., **86**(8), p. 082101.
[22] Pop, E., Sinha, S., and Goodson, K., 2006, "Heat Generation and Transport in Nanometer-Scale Transistors," Proc. IEEE, **94**(8), pp. 1587–1601.
[23] Reissland, J. A., 1973, *The Physics of Phonons*, Wiley-Interscience, New York.
[24] McGaughey, A. J., and Kaviany, M., 2004, "Quantitative Validation of the Boltzmann Transport Equation Phonon Thermal Conductivity Model Under the Single-Mode Relaxation Time Approximation," Phys. Rev. B, **69**(9), p. 094303.
[25] Ladd, A., Moran, B., and Hoover, W. G., 1986, "Lattice Thermal Conductivity: A Comparison of Molecular Dynamics and Anharmonic Lattice Dynamics," Phys. Rev. B, **34**(8), pp. 5058–5064.
[26] Sun, L., and Murthy, J. Y., 2005, "Molecular Dynamics Simulation of Phonon Transport in EDIP Silicon," ASME Paper No. HT2005-72200.
[27] Henry, A. S., and Chen, G., 2008, "Spectral Phonon Transport Properties of Silicon Based on Molecular Dynamics Simulations and Lattice Dynamics," J. Comput. Theor. Nanosci., **5**(2), pp. 141–152.
[28] Turney, J. E., Landry, E. S., McGaughey, A. J. H., and Amon, C. H., 2009, "Predicting Phonon Properties and Thermal Conductivity From Anharmonic Lattice Dynamics Calculations and Molecular Dynamics Simulations," Phys. Rev. B, **79**(6), p. 064301.
[29] Dove, M. T., 1993, *Introduction to Lattice Dynamics*, Cambridge University Press, New York.
[30] Pearson, E. M., Halicioglu, T., and Tiller, W. A., 1985, "Laplace-Transform Technique for Deriving Thermodynamics Equations From the Classical Microcanonical Ensemble," Phys. Rev. A, **32**(5), pp. 3030–3039.
[31] Porter, L. J., Yip, S., Yamaguchi, M., Kaburaki, H., and Tang, M., 1997, "Empirical Bond-Order Potential Description of Thermodynamic Properties of Crystalline Silicon," J. Appl. Phys., **81**(1), pp. 96–106.
[32] Tiwari, M. D., and Agrawal, B. K., 1971, "Analysis of the Lattice Thermal Conductivity of Germanium," Phys. Rev. B, **4**(10), pp. 3527–3532.
[33] Volz, S. G., and Chen, G., 1999, "Molecular Dynamics Simulation of Thermal Conductivity of Silicon Nanowires," Appl. Phys. Lett., **75**(14), pp. 2056–2058.
[34] Gomes, C., Madrid, M., Goicochea, J. V., and Amon, C. H., 2006, "In-Plane and Out-of-Plane Thermal Conductivity of Silicon Thin Films Predicted by Molecular Dynamics," ASME J. Heat Transfer, **128**(11), pp. 1114–1121.
[35] Lee, Y. H., Biswas, R., Soukoulis, C. M., Wang, C. Z., Chan, C. T., and Ho, K. M., 1991, "Molecular-Dynamics Simulation of Thermal Conductivity in Amorphous Silicon," Phys. Rev. B, **43**(8), pp. 6573–6580.
[36] Volz, S. G., and Chen, G., 2000, "Molecular-Dynamics Simulation of Thermal Conductivity of Silicon Crystals," Phys. Rev. B, **61**(4), pp. 2651–2656.
[37] Kremer, R. K., Graf, K., Cardona, M., Devyatykh, G. G., Gusev, A. V., Gibsin, A. M., Inyushkin, A. V., Taldenkov, A. N., and Pohl, H., 2004, "Thermal Conductivity of Isotopically Enriched 28Si: Revisited," Solid State Commun., **131**(8), pp. 499–503.
[38] Murakawa, A., Ishii, H., and Kakimoto, K., 2004, "An Investigation of Thermal Conductivity of Silicon as a Function of Isotope Concentration by Molecular Dynamics," J. Cryst. Growth, **267**(3–4), pp. 452–457.
[39] Carruthers, P., 1961, "Theory of Thermal Conductivity of Solids at Low Temperatures," Rev. Mod. Phys., **33**(1), pp. 92–138.
[40] Goicochea, J. V., Madrid, M., and Amon, C. H., 2009, "Effects of Quantum Corrections and Isotope Scattering on Silicon Thermal Properties," Thermal Investigations of ICs and Systems, THERMINIC, Leuven, Belgium, pp. 197–202.
[41] Goicochea, J. V., 2008, "Hierarchical Modeling of Heat Transfer in Silicon-Based Electronic Devices," Ph.D. thesis, Carnegie Mellon University, Pittsburgh, PA.
[42] Goicochea, J. V., and Michel, B., 2010, "Phonon Relaxation Times of Germanium Determined by Molecular Dynamics at 1000 K," Semiconductor Thermal Measurement, Modeling and Management Symposium (SEMITHERM), Santa Clara, CA.
[43] Desai, P. D., 1986, "Thermodynamic Properties of Iron and Silicon," J. Phys. Chem. Ref. Data, **15**(3), pp. 967–083.
[44] Ho, C. Y., Powell, R. W., and Liley, P. E., 1974, "Thermal Conductivity of the Elements," J. Phys. Chem. Ref. Data, **3**(1), pp. 1–796.
[45] Escobar, R., Smith, B., and Amon, C. H., 2006, "Lattice Boltzmann Modeling of Subcontinuum Energy Transport in Crystalline and Amorphous Microelectronic Devices," ASME J. Electron. Packag., **128**(2), pp. 115–124.
[46] Escobar, R. A., Ghai, S. S., Jhon, M. S., and Amon, C. H., 2006, "Multi-Length and Time Scale Thermal Transport Using the Lattice Boltzmann Method With Applications to Electronics Cooling," Int. J. Heat Mass Transfer, **49**(1–2), pp. 97–107.
[47] Han, Y., and Klemens, P. G., 1993, "Anharmonic Thermal Resistivity of Dielectric Crystals at Low Temperatures," Phys. Rev. B, **48**(9), pp. 6033–6042.
[48] Escobar, R. A., and Amon, C. H., 2008, "Thin Film Phonon Heat Conduction by the Dispersion Lattice Boltzmann Method," ASME J. Heat Transfer, **130**(9), p. 092402.
[49] Succi, S., 2001, *The Lattice Boltzmann Equation for Fluid Mechanics and Beyond*, Clarendon, Oxford, UK.
[50] Qian, Y. H., d'Humieres, D., and Lallemand, P., 1992, "Lattice BGK for Navier-Stokes Equation," Europhys. Lett., **17**(6), pp. 479–484.